



HAL
open science

The Sm-Fe-V based 1:12 bulk magnets

A.M. M Schönhöbel, Rajasekhar Madugundo, A.M. M Gabay, J.M. M Barandiarán, G.C. C Hadjipanayis

► **To cite this version:**

A.M. M Schönhöbel, Rajasekhar Madugundo, A.M. M Gabay, J.M. M Barandiarán, G.C. C Hadjipanayis. The Sm-Fe-V based 1:12 bulk magnets. *Journal of Alloys and Compounds*, 2019, 791, pp.1122-1127. 10.1016/j.jallcom.2019.03.249 . hal-02264183

HAL Id: hal-02264183

<https://hal.science/hal-02264183>

Submitted on 14 Sep 2019

HAL is a multi-disciplinary open access archive for the deposit and dissemination of scientific research documents, whether they are published or not. The documents may come from teaching and research institutions in France or abroad, or from public or private research centers.

L'archive ouverte pluridisciplinaire **HAL**, est destinée au dépôt et à la diffusion de documents scientifiques de niveau recherche, publiés ou non, émanant des établissements d'enseignement et de recherche français ou étrangers, des laboratoires publics ou privés.

The Sm-Fe-V based 1:12 bulk magnets

A. M. Schönhöbel^{a,b}, R. Madugundo^a, A. M. Gabay^c, J. M. Barandiarán^{a,b}, G. C. Hadjipanayis^c

^a*BCMaterials, UPV/EHU Science Park, 48940 Leioa, Spain*

^b*Department of Electricity & Electronics, University Basque Country (UPV/EHU), 48940 Leioa, Spain*

^c*Department of Physics & Astronomy, University of Delaware, Newark, DE, 19716, USA*

Abstract

A bulk magnet based on Sm-Fe-V with the ThMn₁₂ crystal structure has been fabricated for the first time by hot-compaction of mechanically milled powders with a density of 92% of the theoretical density. The isotropic magnet exhibits a maximum coercivity of 1.06 T with a magnetization of 0.59 T, a remanent magnetization of 0.42 T and a $(BH)_{\max}$ of 28 kJ m⁻³ at 3 T applied field. The Curie temperature is found to be 330 °C and the temperature coefficients of remanent magnetization and coercivity are 0.14% C⁻¹ and 0.39% C⁻¹, respectively. Minor hysteresis loops indicate a coercivity mechanism similar to that of the nanocrystalline Nd-Fe-B magnets. The isotropic magnet was hot-deformed up to 75% of its height, and the best magnetic properties obtained were $\mu_0 M_{3T} = 0.63$ T, $\mu_0 M_r = 0.45$ T, $\mu_0 H_c = 0.88$ T and $(BH)_{\max} = 33$ kJ m⁻³. A small texture perpendicular to compaction direction was detected when the amount of vanadium was reduced, and the deformation temperature was increased from 800 to 1000 °C.

Keywords

Permanent magnets, ThMn₁₂, hot-compaction, mechanical milling, anisotropic magnet, hot-deformation

1. Introduction

There is an increasing worldwide demand to minimize dependency on fossil fuels due to sustainability problems along with the drive to reduce carbon emissions by encouraging the use of wind energy and electric/hybrid vehicles. This is going to result in phenomenal increase in demand for high performance permanent magnets (PMs), an industry which is already under pressure due to the high demand, high rare-earth (RE) prices and volatile supply chain of critical metals such as Dy, Tb. In an effort to reduce RE-metals consumption, there has been a renewed interest in 1:12 compounds with ThMn₁₂-type crystal structure (space group *I4/mmm*) [1–4]. These compounds contain only a 7.7% of RE, compared with 11.8% in RE₂Fe₁₄B, and have a tetragonal structure, which is a requirement for uniaxial magnetocrystalline anisotropy (easy *c*-axis for RE=Sm and easy plane for RE=Nd). The uniaxial anisotropy of the Sm-based alloys makes them more suitable as starting materials for producing anisotropic permanent magnets than the Nd-based systems. The REFe₁₂ binary compounds are not thermodynamically stable and do not exist in the bulk alloy form, but can be stabilized by adding a third element such as Ti, V, Mo, Cr, W or Si [5–7]. Intrinsic properties of these alloys have been investigated in depth in view of their interest as potentially suitable for permanent magnets processing [8–13]. The saturation magnetization (M_s), anisotropy field (H_A) and Curie temperature (T_C) of these 1:12 alloys are comparable to those of Nd₂Fe₁₄B. Hard magnetic properties with coercivity ($\mu_0 H_c$) values ranging between 0.2 to 0.78 T were reported in melt-spun ribbons of Sm(Fe,M)₁₂ (M = Ti, Mo, V) alloys [14–17]. Only a couple of studies have been reported on bulk magnets made out of 1:12 alloys. Shultz et al. [18] reported a Sm-Fe-V based resin bonded magnet with 1.17 T of coercivity prepared from the mechanically alloyed powders. Pinkerton et al. [14] reported a bulk magnet produced by hot pressing the Sm_{0.89}Fe₁₀V₂ melt spun ribbons at 850 °C. However, the $\mu_0 H_c$ values obtained in the magnet was only 0.56 T. The main challenge in making a magnet is to obtain 1:12 phase while suppressing the formation of α -(Fe,M) because of the loss of Sm-metal during the various stages of processing due to evaporation and oxidation. Development of high $\mu_0 H_c$ in the alloy powders and optimizing the microstructure of the bulk sample and maintaining it throughout the processing is crucial. In this paper, we are reporting a process we developed to make a bulk magnet by using hot-compaction of mechanically milled powders. Based on the previous reports on the intrinsic and hard magnetic properties of 1:12 compounds, we have chosen the Sm-Fe-V alloy [8,12,14,18–20]. We also report

the thermal stability of $\mu_0 H_c$ and $\mu_0 M_r$ and results on our latest attempts to obtain an anisotropic magnet by hot-deformation.

2. Experimental

Ingots with nominal compositions $\text{Sm}_{12}\text{Fe}_{73}\text{V}_{15}$ and $\text{Sm}_{12}\text{Fe}_{76.5}\text{V}_{11.5}$ were prepared by arc-melting the pure elements Sm (pieces 99.9%), Fe (pieces 99.97%) and V (sheets 99.7%) under Ar atmosphere. Excess of Sm was included in the alloy to prevent the Sm losses. The ingots were annealed in Ar to maximize the volume fraction of the 1:12 phase at different temperatures ranging from 800 to 1100 °C for 2 days and quenched in water. The powders were milled in a SPEX mill unit using a custom-made hardened steel vial equipped with a vacuum valve, and steel balls of 12, 8, 5 and 4 mm diameter under high purity argon. A ball to powder mass of 20:1 was used. The as-milled powders were hot-compacted at 650 °C in vacuum using a tungsten carbide (WC) die by applying a pressure of 220 MPa. For hot-compaction, the sample was heated to 650 °C at a heating rate of 65 °C min⁻¹ and the pressure was applied for 13 min. Finally, the sample was cooled to room temperature and a 92%-dense isotropic magnet was obtained. The hot-compacted sample was then heat-treated at 700 °C for 10 min to 30 min to optimize the coercivity. To obtain an anisotropic magnet, the hot-compacted magnet was placed between alumina punches and then hot-deformed parallel to the press direction at 800 °C. The pieces were hot-deformed up to 75% of their original height.

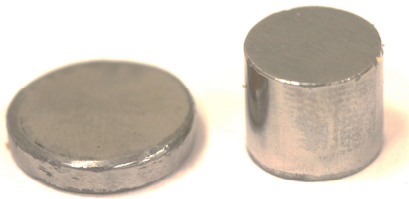


Fig. 1 Sm-Fe-V based 1:12 hot-compacted and hot-deformed magnets

Hysteresis loops were measured with field applied parallel to the deformation direction (//) and the perpendicular direction (\perp). A maximum field of 3 T was applied during the measurements, and the hysteresis loops were corrected for the self-demagnetization effect.

Temperature coefficients of remanence (α), and coercivity (β) in a temperature range from T_1 to T_2 , defined as,

$$\alpha \equiv \frac{M_r(T_2) - M_r(T_1)}{M_r(T_1)} \frac{1}{\Delta T} \times 100\% \quad \text{Eq. (1)}$$

and

$$\beta \equiv \frac{\mu_0 H_c(T_2) - \mu_0 H_c(T_1)}{\mu_0 H_c(T_1)} \frac{1}{\Delta T} \times 100\%, \quad \text{Eq. (2)}$$

were calculated using the expressions,

$$\alpha = \frac{a_r(T_2 + T_1) + b_r}{M_r(T_1)} \quad \text{Eq. (3)}$$

and

$$\beta = \frac{a_c(T_2 + T_1) + b_c}{\mu_0 H_c(T_1)}. \quad \text{Eq. (4)}$$

where a_i and b_i ($i = r, c$) are the regression coefficients of the quadratic functions $M_r(T)$ and $\mu_0 H_c(T)$. The crystal structure was studied by X-ray diffraction (XRD) using a Rigaku Ultima IV instrument with Cu-K α radiation. Lattice parameters and volume fractions of the different phases were calculated using Rietveld analysis [21]. Microstructure studies were performed using a JEOL (JSM- 6335F) scanning electron microscope (SEM).

3. Results and discussion

The XRD patterns of the $\text{Sm}_{12}\text{Fe}_{73}\text{V}_{15}$ sample at different stages of the processing are shown in Fig. 2. The homogenized ingot (Fig. 2(a)) shows reflections from the 1:12 phase (estimated volume fraction 84.9%), REFe_2 Laves phase (1:2) (14.3%) and a small amount of α -(Fe,V) phase (0.8%); this was also confirmed by thermo-magnetic data. With milling, the peaks of both the 1:12 and 1:2 structures become very weak and broad, and after 10 hours of milling, a strong broad peak around 44.3° is observed, along with an almost negligible broad halo peak overlapping the 1:12 and 1:2 peaks, as shown in Fig. 2(b). This indicates the formation of an amorphous phase coexisting with an α -(Fe,V) phase. The small shift from the pure α -Fe diffraction angle ($2\theta = 44.7^\circ$) suggests a lattice expansion, this is a result from the solid solution of V atoms in the Fe-based bcc lattice. The hot-compacted magnet shows the presence of 1:12 and 1:2 phases along with a small amount of Sm oxides (Fig. 2(c)) possibly formed because the as-milled powder

was exposed to the air. The hot-compact sample shows very broad peaks indicating very fine grains. The hot-compact sample subjected to an additional annealing at 700 °C for 30 min shows an XRD pattern with sharper and well-defined peaks compared with the previous stage, indicating an increase in the grain size. Refinement of the XRD patterns show the presence of the 1:12 phase (85.9%), 1:2 (1.6%), SmO (5.2%), Sm₂O₃ (3.8%), Sm (2.6%) and a very small amount of α -(Fe,V) (0.9%). As one can see, the amount of the 1:2 phase is reduced after processing by a 89%, but the initial excess of Sm has prevented loss of the 1:12. The Rietveld refinement parameter can be found in the supplementary data.

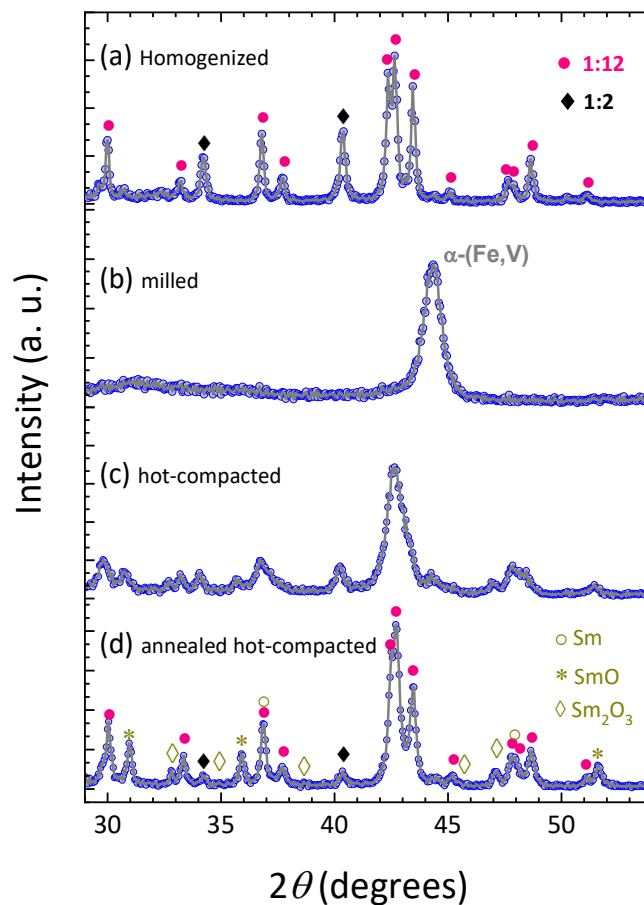


Fig. 2 X-ray diffraction patterns of the $\text{Sm}_{12}\text{Fe}_{73}\text{V}_{15}$ samples (a) homogenized at 800°C (b) after milling (c) hot-compact and (d) annealed hot-compact.

Fig. 3 shows the evolution of the hysteresis loops measured by applying a maximum field of 3 T at room temperature for the homogenized, as milled, hot-compacted and the annealed hot-compacted samples. Table 1 summarizes the values of $\mu_0 H_c$, $\mu_0 M_{3T}$ and $\mu_0 M_r$.

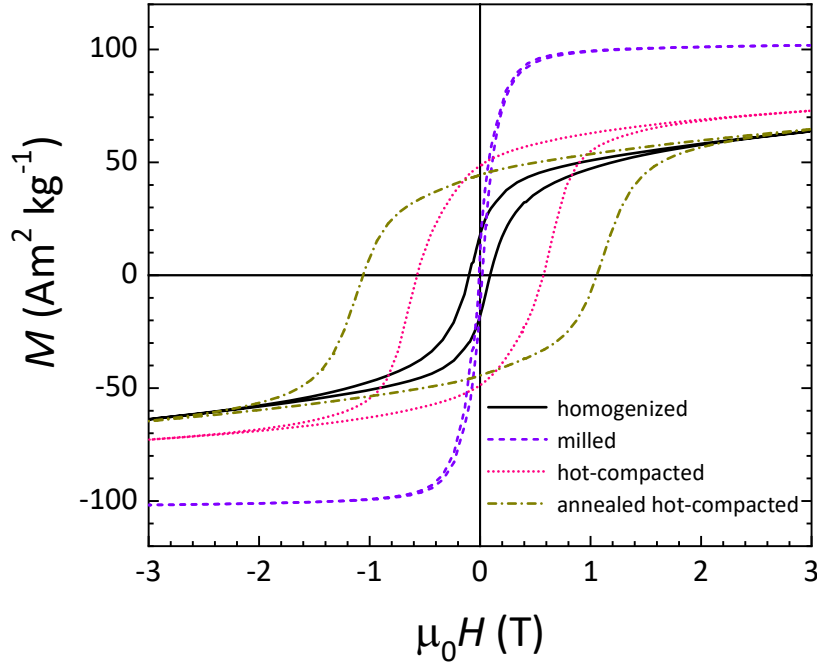


Fig. 3 Hysteresis loops of the $\text{Sm}_{12}\text{Fe}_{73}\text{V}_{15}$ homogenized, after milling for 10 h, hot-compacted and annealed hot-compacted samples.

The homogenized sample shows $\mu_0 H_c$ and $\mu_0 M_{3T}$ of 0.09 T and 0.62 T ($64 \text{ Am}^2 \text{ kg}^{-1}$), respectively. After milling, the value of $\mu_0 M_{3T}$ increases to ($102 \text{ Am}^2 \text{ kg}^{-1}$) and the $\mu_0 H_c$ was measured to be 0.02 T, which is due to the absence of high-anisotropy phase and large volume fraction of the α -(Fe,V) solid solution. Optimal heat-treatment of the hot-compacted magnet results in an increase of $\mu_0 H_c$ to 1.06 T, the highest value reported so far in 1:12 bulk magnets. The $\mu_0 M_{3T}$, $\mu_0 M_r$ and $(BH)_{\text{max}}$ are found to be 0.59 T ($64 \text{ Am}^2 \text{ kg}^{-1}$), 0.42 T ($46 \text{ Am}^2 \text{ kg}^{-1}$) and 28 kJ m^{-3} (3.5 MGOe). The hysteresis loops of the hot-compacted and annealed hot-compacted sample do not show any zero-field steps which could indicate presence of the soft magnetic α -(Fe,V) phase, which is consistent with the XRD results.

We obtained greater coercivity and better loop rectangularity than Pinkerton and Van Wingerden [30] in the only earlier reported fully dense Sm-Fe-V magnet ($\mu_0 H_c = 0.56 \text{ T}$,

$\mu_0 M_r = 0.54$ T in $\text{Sm}_{15}\text{Fe}_{70}\text{V}_{15}$). The improvement may be due to the use of high-energy milling for manufacturing the nanocrystalline precursor material rather than the melt-spinning. Indeed, the coercivity values achieved in this work are similar to those reported by Schultz et al. [18] ($\mu_0 H_c = 1.17$ T, $\mu_0 M_r = 0.49$ T in $\text{Sm}_{15}\text{Fe}_{70}\text{V}_{15}$) who employed mechanical alloying but did not prepare a fully dense magnet. On the other hand, the higher remanence values reported by Ding and Rosenberg [16] for melt-spun Sm-Fe-Co-V alloys indicate that a partial Co substitution for Fe may increase the energy density of the fully dense Sm-Fe-V magnets even in the absence of the crystallographic texture.

Table 1. Magnetic properties of the $\text{Sm}_{12}\text{Fe}_{73}\text{V}_{15}$ sample at different stages of processing. Values of $\mu_0 H_c$, $\mu_0 M_{3T}$ and $\mu_0 M_r$ in the parenthesis are given in $\text{Am}^2 \text{kg}^{-1}$. The value of $(BH)_{\max}$ in parenthesis is given in MGOe.

Stage	$\mu_0 H_c$ (T)	$\mu_0 M_{3T}$ (T)	$\mu_0 M_r$ (T)	$(BH)_{\max}$ (kJ/m^3)
Homogenized	0.09	0.62 (64)	0.25 (26)	4 (0.5)
Milled	0.02	-(102)	-(7)	-
Hot-compacted	0.57	0.64 (74)	0.45 (51)	31 (3.8)
Annealed hot-compacted	1.06	0.59 (64)	0.42 (46)	28 (3.5)

In order to study the coercivity mechanism, the virgin and demagnetization curves are measured and shown in Fig. 4. The virgin magnetization curve shows a susceptibility that increases with the applied field going through a maximum at 0.9 T, a field comparable with the maximum coercivity of the sample, consistent with the fact that the maximum amount of reversals occurs at this field. The susceptibility falls off again as the magnetization is approaching to saturation at high fields. The dependence of coercivity and remanent magnetization on applied field $\mu_0 H_m$, which is determined from the demagnetization curves, are plotted in the inset of Fig 4. The remanent magnetization and coercivity curves show a similar behavior, showing a small initial increase with $\mu_0 H_m$ until $\mu_0 H_m$ becomes comparable to the coercivity, whereupon both $\mu_0 H_c$ and

M_r increase dramatically to saturation. This kind of behavior is characteristic of isotropic hard nanocrystalline materials (like Nd-Fe-B). The mechanisms of domain wall-pinning [21–26] and nucleation of reversed domains cannot be ruled out completely.

Thermomagnetic data measured on the optimally annealed compacted sample, show the T_C of the 1:12 phase to be 330 °C; there is also another minority phase with T_C at 411 °C, which is attributed to the 1:2 phase.

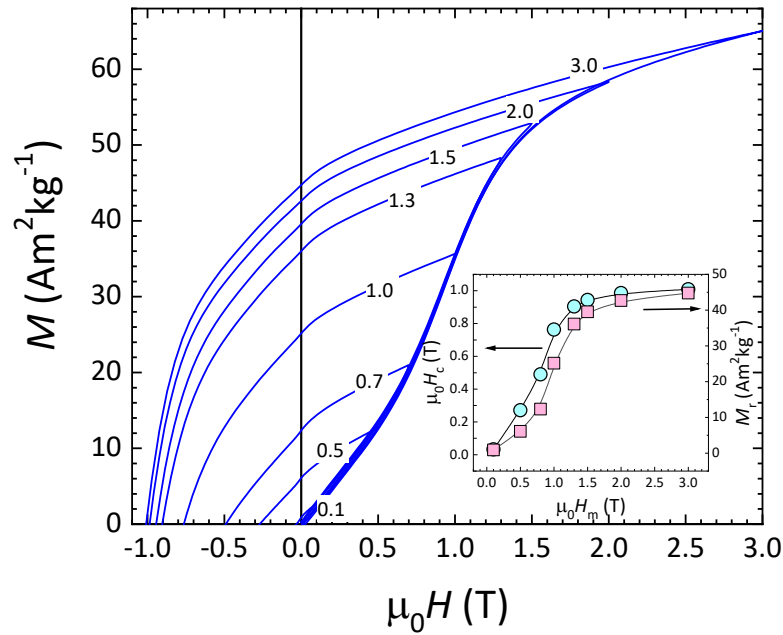


Fig. 4 Virgin and demagnetization curves at room temperature of the annealed hot-compacted $\text{Sm}_{12}\text{Fe}_{73}\text{V}_{15}$ magnet. The field value on each demagnetization curve is the maximum applied field in teslas. The sample was thermally demagnetized before the measurement of each curve.

Fig. 5(a) shows the second quadrant of M-H hysteresis loops at temperatures ranging from 223 to 327 °C for the annealed hot-compacted magnet. The temperature dependence of $\mu_0 M_r$ and $\mu_0 H_c$, are shown in Fig. 5(b). Here, $\mu_0 H_c$ and $\mu_0 M_r$ decreases with increasing temperature, and ultimately the $\mu_0 M_r$ becomes zero at the T_C of the 1:12 phase (330 °C). Similarly, to the Nd-Fe-B magnets [22], the decrease in $\mu_0 H_c$ is more prominent than $\mu_0 M_r$. The values of $\mu_0 H_c$ and $\mu_0 M_r$ are found to be 2.6 T and 0.5 T ($51 \text{ Am}^2 \text{ kg}^{-1}$) at -223 °C and 0.5 T and 0.3 T ($33 \text{ Am}^2 \text{ kg}^{-1}$) at 177 °C, respectively. Temperature coefficients α and β , are calculated using eq. (3) and (4). The

coefficients of the polynomial regressions and r -square are shown in Table 2. The absolute values of a and b at temperature range from 20 °C to 100 °C are 0.14% °C⁻¹ and 0.39% °C⁻¹, respectively. The coefficient b is significantly lower than that of standard Nd-Fe-B sintered or hot-deformed magnets, which is above 0.55% °C⁻¹ [21,22].

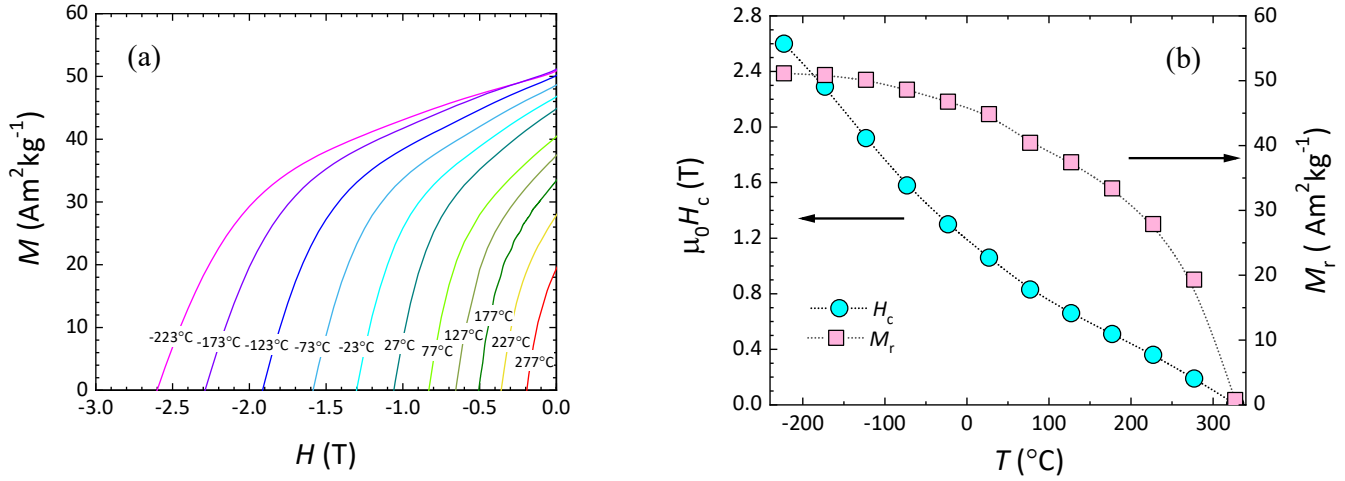


Fig. 5 (a) Demagnetization curves measured at different temperatures and (b) temperature dependence of coercivity and remanence of the annealed hot-compacted $\text{Sm}_{12}\text{Fe}_{73}\text{V}_{15}$ magnet.

Table 2. The coefficients and r -square from the polynomial regression of $M_{r(T)} = a_r T^2 + b_r T + c_r$ and $\mu_0 H_{c(T)} = a_c T^2 + b_c T + c_c$ for temperature range 20-100 °C for the data plotted in Fig. 5(b).

	a_i ($\times 10^{-4}$ °C ⁻²)	b_i (°C ⁻¹)	c_i	r^2
M_r	-1.20 $\text{Am}^2 \text{kg}^{-1}$	-0.0505 $\text{Am}^2 \text{kg}^{-1}$	45.7 $\text{Am}^2 \text{kg}^{-1}$	0.99803
$\mu_0 H_c$	0.0687 T	0.00512 T	1.19 T	0.99964

Fig. 6 shows the SEM secondary-electrons image taken from the fractured surface of the hot compacted magnet. The average grain size of the hot compacted magnet was estimated to be 13 ± 3 nm. The high $\mu_0 H_c$ obtained in this sample could be attributed to the very fine grain size of the highly anisotropic 1:12 phase, also It seems to be that the as-milled structure aids to the formation of a very fine grain microstructure of 1:12 phase during the hot-compaction.

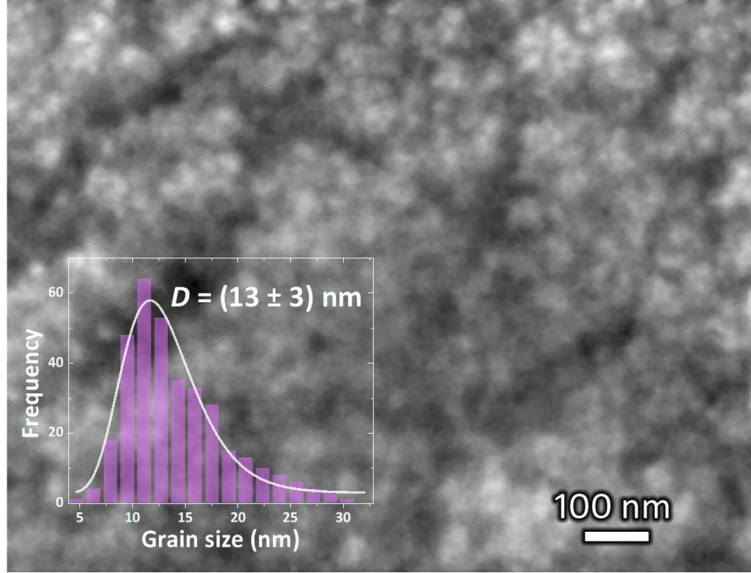


Fig. 6. SEM secondary electrons-image of the fractured surface of the hot-compacted $\text{Sm}_{12}\text{Fe}_{73}\text{V}_{15}$ magnet.

Hysteresis loops of $\text{Sm}_{12}\text{Fe}_{73}\text{V}_{15}$ and $\text{Sm}_{12}\text{Fe}_{76.5}\text{V}_{11.5}$ hot deformed magnets measured parallel (\parallel) and perpendicular (\perp) to the compression direction ΔL are shown in Fig 7(a) and 7(b), respectively. The magnetic properties are listed in Table 3. After deformation of $\text{Sm}_{12}\text{Fe}_{73}\text{V}_{15}$ sample at $800\text{ }^\circ\text{C}$, $\mu_0 M_{3T}$ remains almost unchanged at 0.63 T ($66.4\text{ Am}^2\text{ kg}^{-1}$) and the $\mu_0 H_c$ is increased to 0.88 T compared with the hot-compacted magnet. An $\mu_0 M_r$ value of 0.45 T ($47\text{ Am}^2\text{ kg}^{-1}$) and 0.42 T ($44\text{ Am}^2\text{ kg}^{-1}$) are obtained when the hysteresis loops were measured with field applied \perp and \parallel directions, respectively, indicating a small degree of anisotropy (DOA) development in the plane perpendicular to the deformation, this is in contrary to that of $\text{Nd}_2\text{Fe}_{14}\text{B}$ based hot-deformed magnets, where the c -axis of grains aligns along the press direction [23,24]. The DOA was calculated using the formula $\text{DOA} = (\mu_0 M_r^\perp - \mu_0 M_r^\parallel) / \mu_0 M_r^\perp$, where $\mu_0 M_r^\perp$ is the remanence measured \perp to the deformation and $\mu_0 M_r^\parallel$ measured \parallel to the deformation. The deformed magnet shows a DOA value of 0.095 . The $\mu_0 M_r$ and $(BH)_{\max}$ of 0.45 T ($47\text{ Am}^2\text{ kg}^{-1}$) and 33 kJ/m^3 (4.1 MGOe) were obtained from the hysteresis loop measured in \perp direction. When V is reduced from 15 to 11.5 at.%, and the $\text{Sm}_{12}\text{Fe}_{76.5}\text{V}_{11.5}$ isotropic hot-compacted magnet is deformed at $1000\text{ }^\circ\text{C}$ (see Fig. 7(b)), there is a noticeable increase in the DOA to 0.286 resulting in $\mu_0 M_r^\perp$ of 0.47 T ($52\text{ Am}^2\text{ kg}^{-1}$) and $\mu_0 H_c$ of 0.41 T . The XRD results indicate that the recrystallization is completed, and grain growth takes place during the exposure to the high deformation temperature.

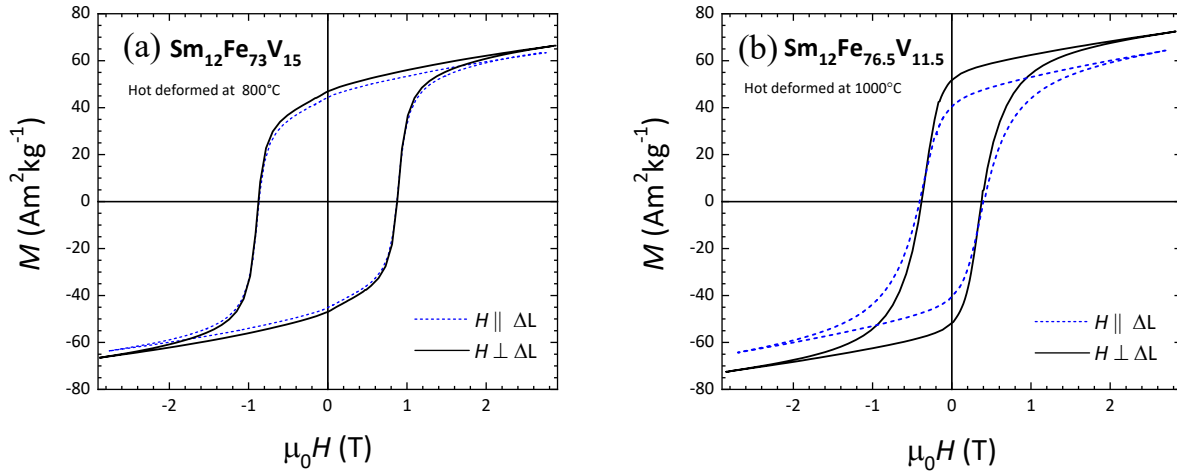


Fig. 7: Hysteresis loops of the hot-deformed magnet measured parallel (\parallel) and perpendicular (\perp) to the deformation (a) $\text{Sm}_{12}\text{Fe}_{73}\text{V}_{15}$ (b) $\text{Sm}_{12}\text{Fe}_{76.5}\text{V}_{11.5}$.

Table 3. Magnetic properties of $\text{Sm}_{12}\text{F}_{73}\text{V}_{15}$ and $\text{Sm}_{12}\text{F}_{76.5}\text{V}_{11.5}$ deformed magnets. Values in parenthesis are given in $\text{Am}^2\text{kg}^{-1}$. The value of $(BH)_{\text{max}}$ in parenthesis is given in MGOe.

Magnet	T_{deform} ($^\circ\text{C}$)	$\mu_0 M_r^\perp$ (T)	$\mu_0 M_r^\parallel$ (T)	DOA	$\mu_0 H_c$ (T)	$(BH)_{\text{max}}$ (kJ/m^3)
$\text{Sm}_{12}\text{F}_{73}\text{V}_{15}$	800	0.45 (47)	0.42 (44)	0.095	0.88	33 (4.1)
$\text{Sm}_{12}\text{F}_{76.5}\text{V}_{11.5}$	1000	0.47 (52)	0.37 (40)	0.286	0.41	29 (3.7)

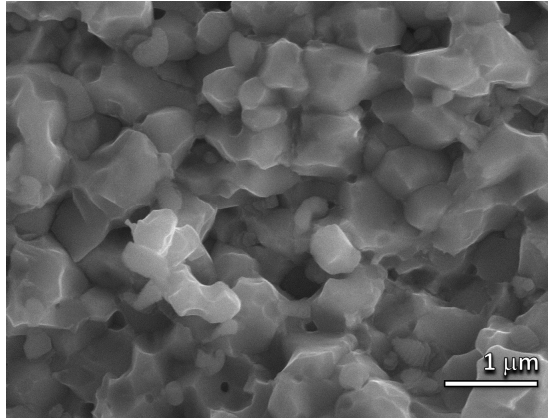


Fig. 8. Microstructure of $\text{Sm}_{12}\text{Fe}_{76.5}\text{V}_{11.5}$ magnet deformed at 1000 °C.

Much larger grains, ranging between 0.3 μm and 1 μm , are observed (Fig. 8), which explain the markedly lower $\mu_0 H_c$ of 0.41 T. Although texture is evident from the magnetic measurements, the 1:12 grains maintain a nearly equiaxed morphology (unlike, for example, the $\text{Nd}_2\text{Fe}_{14}\text{B}$ grains in the hot-deformed Nd-Fe-B magnets [25]). The texture is similar to that of observed in Mn-Al hot-deformed magnets [26,27]. The magnets developed in this study exhibit optimal magnetic properties in every direction perpendicular to the deformation direction. These magnets are suitable for motor-generator applications where circumferential multipole magnets are used. In 1:12 magnets, uniaxial texture may be possible by hot-extrusion as it was obtained in the case of Mn-Al magnets [28,29].

Conclusions

We have succeeded in fabricating, for the first time, a bulk $\text{Sm}(\text{Fe},\text{V})_{12}$ based nanocrystalline magnet by hot-compaction of mechanically milled powders, with a $\mu_0 H_c = 1.06$ T and $(BH)_{\text{max}} = 28$ kJ m^{-3} . The T_C was 330 °C and the temperature coefficients $\alpha = 0.14\%$ C^{-1} and $\beta = 0.39\%$ C^{-1} . The β value is comparatively lower than that of NdFeB magnets. A texture perpendicular to the deformation direction was observed. This kind of behavior is different from that of die-upset Nd-Fe-B magnets and would indicate the use of hot extrusion rather than die-upsetting for the development of bulk magnets. These results encourage the study on highly

textured ultrafine-grained magnets, reopening the development of 1:12 Sm-based anisotropic magnets.

Acknowledgements

This work was supported by the Novamag and Inapem projects under EU Horizon 2020 Programme (grants 686056 and 691235) and the U.S. Department of Energy (DOE DE-FG02-90ER45413).

References

- [1] I.S. Tereshina, N. V. Kostyuchenko, E.A. Tereshina-Chitrova, Y. Skourski, M. Doerr, I.A. Pelevin, A.K. Zvezdin, M. Paukov, L. Havela, H. Drulis, ThMn₁₂-type phases for magnets with low rare-earth content: Crystal-field analysis of the full magnetization process, *Sci. Rep.* 8 (2018) 8–13. doi:10.1038/s41598-018-21756-5.
- [2] Y. Hirayama, Y.K. Takahashi, S. Hirosawa, K. Hono, *Scripta Materialia* Intrinsic hard magnetic properties of Sm(Fe_{1-x}Co_x)₁₂ compound with the ThMn₁₂ structure, *Scr. Mater.* 138 (2017) 62–65. doi:10.1016/j.scriptamat.2017.05.029.
- [3] A.M. Gabay, R. Cabassi, S. Fabbri, F. Albertini, G.C. Hadjipanayis, Structure and permanent magnet properties of Zr_{1-x}R_xFe₁₀Si₂ alloys with R = Y, La, Ce, Pr and Sm, *J. Alloys Compd.* 683 (2016) 271–275. doi:10.1016/j.jallcom.2016.05.092.
- [4] S. Suzuki, T. Kuno, K. Urushibata, K. Kobayashi, N. Sakuma, K. Washio, M. Yano, A. Kato, A. Manabe, A new magnet material with ThMn₁₂ structure: (Nd_{1-x}Zr_x)(Fe_{1-y}Co_y)_{11+z}Ti_{1-z}N_α (α=0.6-1.3), *J. Magn. Magn. Mater.* 401 (2016) 259–268. doi:10.1016/j.jmmm.2015.10.042.
- [5] K.H.J. Buschow, Permanent magnet materials based on tetragonal rare earth compounds of the type RFe_{12-x}M_x, *J. Magn. Magn. Mater.* 100 (1991) 79–89. doi:10.1016/0304-8853(91)90813-P.
- [6] A.M. Gabay, G.C. Hadjipanayis, Recent developments in RFe₁₂-type compounds for permanent magnets, *Scr. Mater.* 154 (2018) 284–288. doi:10.1016/j.scriptamat.2017.10.033.
- [7] R. Madugundo, N.V.R. Rao, A.M. Schönhöbel, D. Salazar, A. A. El-Gendy, Recent Developments in Nanostructured Permanent Magnet Materials and Their Processing Methods, in: A. El-Gendy, J.M. Barandiaran, R.L. Hadimani (Eds.), *Magn. Nanostructured Mater. From Lab to Fab*, 1st ed., Elsevier, Amsterdam, Netherlands, 2018: pp. 157–198.
- [8] F.R. De Boer, Y.-K. Huang, D.B. De Mooij, K.H.J. Buschow, Magnetic properties of a series of novel ternary intermetallics (RFe₁₀V₂), *J. Less Common Met.* 135 (1987) 199–204. doi:10.1016/0022-5088(87)90481-4.
- [9] K.H.J. Buschow, D.B. de Mooij, M. Brouha, H.H. Smit, R.C. Thiel, Magnetic properties of ternary Fe-rich rare earth intermetallic compounds, *IEEE Trans. Magn.* 24 (1988) 1611–1616. doi:10.1109/20.11547.
- [10] K. Ohashi, Y. Tawara, R. Osugi, J. Sakurai, Y. Komura, Identification of the intermetallic compound consisting of Sm, Ti, Fe, *J. Less Common Met.* 139 (1988) L1–L5. doi:10.1016/0022-5088(88)90020-3.
- [11] Y. Wang, G.C. Hadjipanayis, A. Kim, N.C. Liu, D.J. Sellmyer, Magnetic and structural studies in Sm-Fe-Ti magnets, *J. Appl. Phys.* 67 (1990) 4954–4956. doi:10.1063/1.344745.
- [12] Y.Z. Wang, G.C. Hadjipanayis, Effect of nitrogen on the structural and magnetic properties of intermetallic compounds with the ThMn₁₂ structure, *J. Appl. Phys.* 70 (1991)

6009–6011. doi:10.1063/1.350076.

- [13] P. Tozman, H. Sepehri-Amin, Y.K. Takahashi, S. Hirosawa, K. Hono, Intrinsic magnetic properties of $\text{Sm}(\text{Fe}_{1-x}\text{Co}_x)_{11}\text{Ti}$ and Zr-substituted $\text{Sm}_{1-y}\text{Zr}_y(\text{Fe}_{0.8}\text{Co}_{0.2})_{11.5}\text{Ti}_{0.5}$ compounds with ThMn_{12} structure toward the development of permanent magnets, *Acta Mater.* 153 (2018) 354–363. doi:10.1016/j.actamat.2018.05.008.
- [14] F.E. Pinkerton, D.J. Van Wingerden, Magnetic hardening of $\text{SmFe}_{10}\text{V}_2$ by melt-spinning, *IEEE Trans. Magn.* 25 (1989) 3306–3308. doi:10.1109/20.42285.
- [15] M. Okada, K. Yamagishi, M. Homma, High Coercivity in Melt-Spun $\text{SmFe}_{10}(\text{TiV})_2$ Ribbons, *Mater. Trans. JIM.* 30 (1989) 374–377. doi:10.2320/matertrans1989.30.374.
- [16] J. Ding, M. Rosenberg, Magnetic hardening of melt-spun and crystallized Sm-Fe-V and Sm-(Fe, Co)-V alloys, *J. Less-Common Met.* 161 (1990) 369–374. doi:10.1016/0022-5088(90)90049-P.
- [17] J. Wecker, M. Katter, K. Schnitzke, L. Schultz, Magnetic hardening of Sm-Fe-Ti alloys, *J. Appl. Phys.* 67 (1990) 4951–4953. doi:10.1063/1.344744.
- [18] L. Schultz, K. Schnitzke, J. Wecker, High coercivity in mechanically alloyed Sm-Fe-V magnets with a ThMn_{12} crystal structure, *Appl. Phys. Lett.* 56 (1990) 868–870. doi:10.1063/1.102662.
- [19] K. Ohashi, Y. Tawara, R. Osugi, M. Shimao, Magnetic properties of Fe-rich rare-earth intermetallic compounds with a ThMn_{12} structure, *J. Appl. Phys.* 64 (1988) 5714–5716. doi:10.1063/1.342235.
- [20] J. Yang, S. Dong, Y. Yang, B. Cheng, Structural and magnetic properties of $\text{RFe}_{10.5}\text{V}_{1.5}\text{N}_x$, *J. Appl. Phys.* 75 (1994) 3013–3016. doi:10.1063/1.356168.
- [21] H.M. Rietveld, A profile refinement method for nuclear and magnetic structures, *J. Appl. Crystallogr.* 2 (1969) 65–71. doi:10.1107/S0021889869006558.
- [22] B.M. Ma, W.L. Liu, Y.L. Liang, D.W. Scott, C. Bounds, Comparison of the improvement of thermal stability of NdFeB sintered magnets: Intrinsic and / or microstructural, *J. Appl. Phys.* 75 (1994) 6628–6630.
- [23] H.T. Kim, Y.B. Kim, H.S. Kim, Magnetic properties and texture of NdFeB magnets fabricated by current-applied-pressure-assisted process, *J. Magn. Magn. Mater.* 224 (2001) 173–179. doi:10.1016/S0304-8853(01)00018-X.
- [24] K. Khlopkov, O. Gutfleisch, R. Schäfer, D. Hinz, K.H. Müller, L. Schultz, Interaction domains in die-upset NdFeB magnets in dependence on the degree of deformation, *J. Magn. Magn. Mater.* 272–276 (2004) 2003–2005. doi:10.1016/j.jmmm.2003.12.1102.
- [25] R. Lee, E. Brewer, N. Schaffel, Processing of Neodymium-Iron-Boron melt-spun ribbons to fully dense magnets, *IEEE Trans. Magn.* 21 (1985) 1958–1963. doi:10.1109/TMAG.1985.1064031.
- [26] R. Madugundo, G.C. Hadjipanayis, Anisotropic Mn-Al-(C) hot-deformed bulk magnets, *J. Appl. Phys.* 119 (2016) 013904. doi:10.1063/1.4939578.

- [27] Y. Sakamoto, A. Ibata, S. Kojima, T. Ohtani, New MnAlC permanent magnets exhibiting macroscopically-plane magnetic-anisotropy, *IEEE Trans. Magn.* 16 (1980) 1056–1058. doi:10.1109/TMAG.1980.1060672.
- [28] T. Ohtani, N. Kato, S. Kojima, K. Kojima, Y. Sakamoto, I. Konno, M. Tsukahara, T. Kubo, Magnetic properties of Mn-Al-C permanent magnet alloys, *IEEE Trans. Magn.* 13 (1977) 1328–1330. doi:10.1109/TMAG.1977.1059574.
- [29] J. Thielsch, F. Bittner, T.G. Woodcock, Magnetization reversal processes in hot-extruded τ -MnAl-C, *J. Magn. Magn. Mater.* 426 (2017) 25–31. doi:10.1016/j.jmmm.2016.11.045.
- [30] F.E. Pinkerton, D.J. Van Wingerden, Magnetization process in rapidly solidified neodymium-iron-boron permanent magnet materials, *J. Appl. Phys.* 60 (1986) 3685–3690. doi:10.1063/1.337576.